



Article

Toward a New Generation of Compact Transportable Yb⁺ Optical Clocks

Ksenia Khabarova ^{1,2} , Denis Kryuchkov ^{1,2}, Alexander Borisenko ^{1,2}, Ilia Zalivako ^{1,2} , Ilya Semerikov ^{1,2}, Mikhail Aksenov ^{1,2}, Ivan Sherstov ³, Timur Abbasov ³, Anton Tausenev ⁴ and Nikolay Kolachevsky ^{1,2*}

¹ P.N. Lebedev Physical Institute of the Russian Academy of Science, Leninskiy Prospect 53, 119991 Moscow, Russia

² Russian Quantum Center, Bolshoy Bulvar, 30 Bld. 1, 121205 Moscow, Russia

³ Skolkovo Institute of Science and Technology, 121205 Moscow, Russia

⁴ Avesta Ltd., Fizicheskaya, 11, 108840 Troick, Russia

* Correspondence: kolachevsky@lebedev.ru

Abstract: Optical atomic clocks are currently one of the most sensitive tools making it possible to precisely test the fundamental symmetry properties of spacetime and Einstein's theory of relativity. At the same time, the extremely high stability and accuracy of compact transportable optical clocks open new perspectives in important fields, such as satellite navigation, relativistic geodesy, and the global time and frequency network. Our project aimed to develop a compact transportable optical clock based on a single ytterbium ion. We present the first prototype of the Yb⁺ clock (298 kg in 1 m³) and present several solutions aimed to improve the clock's robustness to approach the demands of a space-qualified system. We present spectroscopic studies of a 435.5 nm quadrupole clock transition with Fourier-limited spectra of 25 Hz. The estimated instability of the output frequency at 1 GHz, which was down-converted with an optical frequency comb (OFC), is at the level of $9 \times 10^{-15} / \sqrt{\tau}$, and the long-term instability and inaccuracy are at the level of 5×10^{-16} . As the next steps, we present a new design for the clock laser and the OFC.

Keywords: ¹⁷¹Yb⁺; transportable optical clock; spectroscopy; quadrupole transition; optical frequency comb



Citation: Khabarova, K.; Kryuchkov, D.; Borisenko, A.; Zalivako, I.; Sherstov, I.; Aksenov, M.; Sherstov, I.; Abbasov, T.; Tausenev, A.; Kolachevsky, N. Toward a New Generation of Compact Transportable Yb⁺ Optical Clocks. *Symmetry* **2022**, *14*, 2213. <https://doi.org/10.3390/sym14102213>

Academic Editor: Wiesław Leonski

Received: 30 September 2022

Accepted: 14 October 2022

Published: 20 October 2022

Publisher's Note: MDPI stays neutral with regard to jurisdictional claims in published maps and institutional affiliations.



Copyright: © 2022 by the authors. Licensee MDPI, Basel, Switzerland. This article is an open access article distributed under the terms and conditions of the Creative Commons Attribution (CC BY) license (<https://creativecommons.org/licenses/by/4.0/>).

1. Introduction

The idea of using narrow optical atomic transitions for the new generation of precise frequency standards appeared shortly after the invention of the laser. Nikolay Basov, whose 100-year anniversary will be celebrated this year, was awarded the Nobel Prize in Physics for his development of the basic principles of masers and lasers. Being at the origin of the maser and laser invention, Basov envisioned lasers' key applications, including optical frequency standards. Remarkably, most of his ideas have not only come to fruition but are actively used in modern developments.

In his review [1], Basov focused on two key problems that were confronting researchers at that time regarding the development of optical atomic clocks. First, a laser with an ultrastable output frequency must be at the heart of any optical clock. Second, one should learn how to accurately measure optical frequencies. Over the past 60 years, these problems have been successfully solved, leading to the next generation of Nobel Prizes. The optical atomic clocks reached an unprecedented level of relative instability and inaccuracy at 10^{-18} [2–4] and are widely used in fundamental and applied research.

Today, atomic clocks occupy an important place in daily life. National frequency scales (UTC, TAI) rely on the operation of atomic clocks, which plays a decisive role in communication technologies, supports network synchronization and provides navigation satellite systems with reference signals. Atomic clocks are widely used in precision physical tests and delicate experiments, such as searching for the drift of fundamental constants, testing for

the Lorentz invariance, searching for dark matter and many others. Theoretical assumptions that the local Lorentz covariance may not be an exact symmetry at all in energies up to the Planck energy and its violation in various models of quantum gravity [4] have motivated strong interest in improving tests for Lorentz symmetry. Experiments involving precision spectroscopy of strongly forbidden atomic transitions have made a significant contribution to the verification of the Lorentz invariance in the electronic sector [5,6]. One remarkable experiment that is mentioned is the $^{171}\text{Yb}^+$ optical clock comparison for Lorentz-symmetry testing [3]. Two single-ion optical clocks demonstrated agreement at the 10^{-18} level over a six-month comparison period, which made it possible to deduce stringent limits of the order of 10^{-21} on the parameters of the Lorentz-symmetry violation.

Since the invention of the optical frequency comb (OFC) [7], optical clocks have been incorporated into national time scales competing with microwave ones (Cs fountains, masers). Until recently, most optical clocks were stationary laboratory-size systems.

Advances in laser technologies, the development of all-fiber OFCs, significant progress in the trapping and laser cooling of atoms and ions and new ideas about how to minimize the contribution of systematic frequency shifts have paved the way to make relatively compact and robust systems. The past decade is highlighted by the development of several transportable optical clocks [8–10] that demonstrate significantly better characteristics than their closest competitors: active masers and the transportable Cs fountain FOM1 [11]. Transportable systems have paved the way for new applications, e.g., relativistic geodesy [12,13]. The Tokyo experiments with two transportable Sr lattice clocks [10] already demonstrated parity with the best traditional geodesic methods. Very recently, gravity time dilation at the millimeter scale was measured by Sr optical clocks at JILA, USA [14,15].

This makes optical clocks one of the most sensitive quantum gravitational sensor perspectives for further testing of general relativity theory.

Several scientific groups are developing increasingly compact and reliable optical clocks suitable for outdoor applications. A group from PTB, Germany, demonstrated the operation of an ^{87}Sr optical lattice clock with a 7.4×10^{-17} frequency uncertainty measured at 698 nm [16]. This system was used for the first on-field chronometric leveling measurement campaign, which aimed to determine the gravitational redshift between the laboratory clocks at INRIM (Turin) and the transportable clock moved to the Modane underground laboratory [13]. A group from RIKEN, Japan, reported on the development of a transportable ^{87}Sr -based optical lattice clock with a fractional uncertainty of 5.5×10^{-18} that was brought to a broadcasting tower for gravitational redshift measurements [10].

Optical lattice clocks benefit from a large number of interrogated atoms, which naturally reduces the frequency instability. Still, optical lattice clocks require a complex loading scheme from a Zeeman slower or a 2D magneto-optical pre-loading trap. The optical trap is shallow, needs accurate adjustments and is sensitive to vibrations. The optical system must typically provide two-stage laser cooling with three pairs of laser beams, a Zeeman slower beam and a powerful laser field for the optical lattice. In turn, a single-ion optical clock based on a very deep 3D Paul trap provides an ion lifetime of up to several months via a simple loading system. It also reduces the Dick effect coming from the periodic clock's operation. Typically, ion optical clocks based on simpler optics than lattice ones require less optical power and are less sensitive to vibrations. The successful development of the Ca^+ optical clock was demonstrated by a group from WIPM, China [17]. The system demonstrates a fractional frequency uncertainty of 7.8×10^{-17} (at the optical carrier) and fits a volume of 0.54 m^3 without the OFC.

Despite significant progress, the optical clock technology is still insufficiently mature for space applications. There are several proposals aimed at optical clock operation in space, e.g., SAGAS [18], EGE [19] and the ESA's SOC2 project based on Sr and Yb optical lattice clock technologies [20]. At the moment, laboratory tests of the clock modules are being carried out, but the launch is scheduled no earlier than 2038.

We have developed a compact single-ion $^{171}\text{Yb}^+$ transportable optical clock system. The project was supported by the Russian Ministry of Science and Higher Education and

the Russian Space Agency. The first prototype was supposed to be less than 300 kg in weight and have a volume of less than 1 m^3 , including the OFC and electronics. The clock operates on a quadrupole transition at 435.5 nm. The ytterbium-171 ion has a relatively simple electronic structure and two well-characterized clock transitions. It is possible to operate both transitions to reduce several systematic shifts (AC Stark shift) to reach excellent metrological characteristics [21].

We report the first prototype of a compact transportable $^{171}\text{Yb}^+$ optical clock and its characteristics. It is designed as several nearly independent modules that can be characterized individually. Several ideas and technical solutions for the envisioned space tests in the 2030s are also discussed.

2. First Generation of a Transportable $^{171}\text{Yb}^+$ Clock at the Lebedev Institute

The first prototype of a compact single $^{171}\text{Yb}^+$ ion clock is designed for transportation in a van and a quick start. The physical package is divided into two vertical racks; one rack contains the optic and mechanical parts, and the second rack contains the electronics (see Figure 1). This configuration provides easy access to all system modules and minimizes heating and perturbation of the optical part by electronic blocks. The optical part consists of four modules: a compact ion package, a clock laser module, cooling and manipulation lasers and an OFC module. Each module is located on a separate breadboard and can be removed from the rack if necessary.



Figure 1. The first generation of a transportable single $^{171}\text{Yb}^+$ clock at the Lebedev Institute.

The optical rack is placed on an active vibration isolation platform. At the rack's bottom, we placed a vacuum chamber containing a Paul trap and a detection system. A weak Yb atomic beam is produced by heating a chunk of metal (natural isotope abundance) placed in an atomic oven. An ion is loaded into a radio-frequency Paul trap via two-step photoionization. The laser at 398.8 nm drives the $^1S_0 \rightarrow ^1P_1$ transition, while the cooling laser at 369 nm ionizes the atom from the upper 1P_1 level. The method is isotope-selective. All required wavelengths for $^{171}\text{Yb}^+$ photoionization, cooling and re-pumping are generated from home-built diode lasers [22], which are frequency stabilized using the wavelength meter Angstrom WS8-10. All laser systems (except the clock laser) are mounted on a breadboard, and radiation is delivered to the trap by optical fibers. The clock laser and auxiliary 1550 laser are mounted on a separate breadboard and located in the middle of the optical rack. Both lasers are frequency stabilized to high-finesse optical cavity modes using the Pound–Drever–Hall technique [23]. The optical part of the frequency comb is mounted at the top of the optical rack.

3. Results

3.1. Ion Trap

An important part of an ion optical clock is the ion trap (see Figure 2). For trapping a single ytterbium ion, a three-dimensional quadrupole Paul trap is used. The trap provides a deep confining potential over all three coordinates by an RF field. After Doppler cooling, the ion is localized in the central region where the RF electric field vanishes, thereby canceling the perturbation of the ion energy levels by the field. The confining field is produced by two RF end-shaped electrodes and two DC cup-shaped electrodes. The electrodes are made of gold-plated titanium (thickness of 10 μm), which exceeds the skin-layer depth at the trap operating frequency (16 MHz). Static external electric fields can push out the ion from the confining potential's zero-point and perturb the clock transition such that four electrodes are used for compensation. The DC potential can be applied independently to each cup-shaped electrode and two atomic ovens. The Paul trap provides a means to achieve the secular frequency up to $2\pi \times 1.15$ MHz [24].

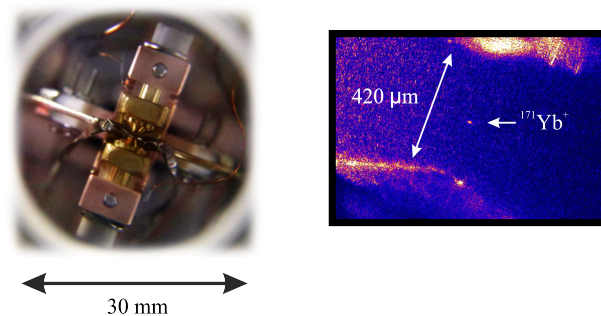


Figure 2. Three-dimensional Paul trap and ion image made by the EMCCD camera.

3.2. Clock Laser

The clock laser module is one of the most important and sensitive elements of an optical clock. We designed the first prototype to be compact and robust in order to fit the target weight and size parameters while maintaining its performance, i.e., keeping its linewidth on the order of several Hz and low-frequency drift. The required 435 nm for quadrupole clock transition spectroscopy is produced by a frequency doubling of the 871 nm laser radiation of the ECDL home-built laser. The laser head has an outer size of $46 \times 46 \times 36$ mm and is constructed in the Littrow configuration (Figure 3). The laser diode mount and laser head housing are thermally stabilized.

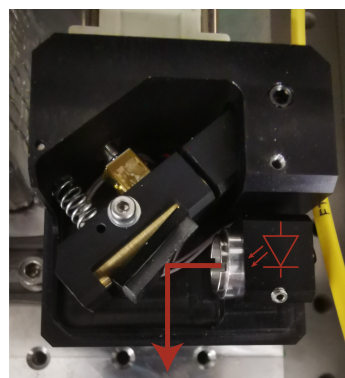


Figure 3. The home-built clock laser head.

The clock laser is stabilized to a 77.5 mm long reference cavity (the body is made of Corning ©ULE glass, and the substrates are made of fused silica), similar to our previous-generation laser systems. The cavity body's geometry is similar to the one described in [25]. The accurate calculation of the Brownian thermal noise [26] for this configuration predicts

the limit on the fractional frequency instability to be less than 8×10^{-16} . The finesse of the cavity is 120,000, which corresponds to a mode linewidth (FWHM) of 16 kHz. The cavity transmission appears to be 0.3% even at the optimal mode-matching due to high losses on the mirrors coated at the Lebedev Institute.

The vacuum chamber was designed for a significant reduction in the size and mass of the system and is similar to that described in [27]. It has three thermal shields for cavity thermal isolation and the suppression of temperature gradients. The cavity mount is also similar to those described in [27] and provides the lowest vibration sensitivity only for the vertical direction. A vacuum of 4×10^{-8} mbar is provided by two 31/s getter pumps produced by the Vremya-Ch company. The resulting mass and volume of the assembled vacuum chamber are reduced to 7 kg and 3.5 L, respectively.

The clock laser module is schematically shown in Figure 4. It is assembled with half-inch optics to provide a further mass-dimensional decrease. The radiation of the ECDL laser with a power of 80 mW and a wavelength of 871 nm is sent to the 60-dB optical isolator to suppress back-reflected light. Then, the spatial profile of the beam is corrected by an anamorphic prism pair and split into three parts.

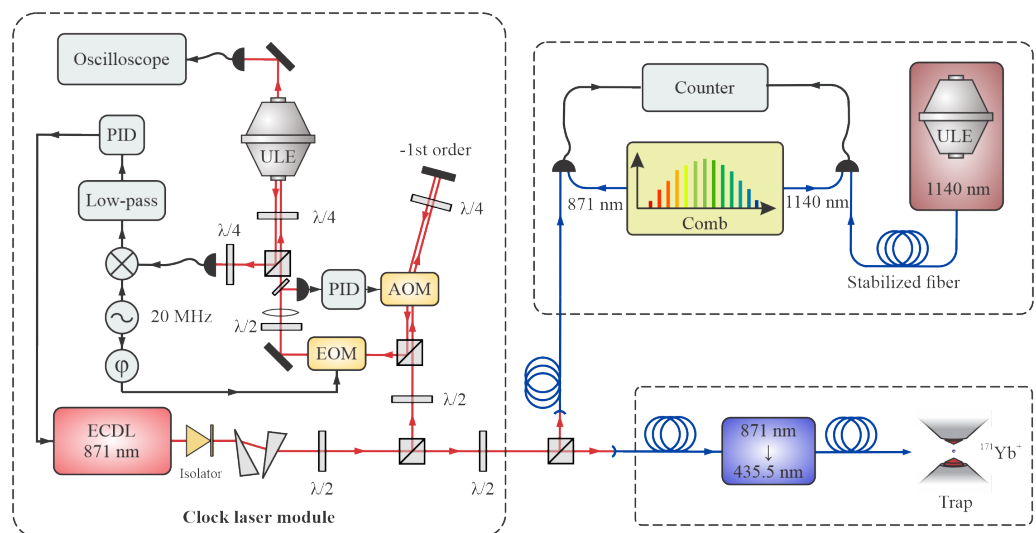


Figure 4. Scheme of clock laser module. PID — fast proportional–integral–derivative controller; ULE — reference optical cavity in a vacuum chamber; AOM, EOM — acousto- and electro-optical modulators; $\lambda/2$ — zero-order half-wave plate;

One part of the laser radiation is sent directly to the fiber-coupled frequency doubler AdvR WSHK0436-P85P40AL3, which provides an output signal of 500 μ W at a wavelength of 435.5 nm for clock transition spectroscopy.

Another part is used for frequency stabilization according to the cavity eigenmode. At first, radiation is sent to the acousto-optical modulator (AOM) in the double-pass configuration. This scheme makes it possible to enlarge the frequency shift and tuning range, which makes the system more useful for spectroscopy by helping to avoid beam displacement during frequency scanning and to suppress additional parasitic etalons.

A third part is sent to the frequency comb. To determine the clock laser's frequency instability, the frequency comb was stabilized to a ^{169}Tm clock laser at 1140 nm [28]. Radiation from both lasers was sent to the frequency comb by optical fibers and mixed by means of balanced heterodyning [29].

The optical path length in the fiber was additionally stabilized to avoid temperature drift and acoustic disturbance [30]. The beat signal was detected by the zero-dead-time counter K+K FXE, which worked in the averaging Lambda regime. The frequency drift of the laser system was found to be $348 \pm 2 \text{ MHz s}^{-1}$. The temperature of the cavity was stabilized to a previously measured [27] zero-CTE point at 10.8 $^{\circ}\text{C}$.

The offset frequency of the frequency comb was stabilized to its repetition rate, while the repetition rate was stabilized to the beat signal between an 1140 nm laser system and the corresponding spectral component of the comb. The beat signal between the stabilized optical comb and an 871 nm laser system was detected by the K+K counter. The signal was recorded with a gate time of 100 ms for a total averaging time of 10,000 s. The data were analyzed using a modified Allan deviation; the result is presented in Figure 5. Since there is no correlation between the frequency noise of the laser systems and the comb's intrinsic noise does not exceed 9×10^{-18} [27], the resulting Allan deviation is $\sigma_{beat} = \sqrt{\sigma_{Yb}^2 + \sigma_{Tm}^2}$, where σ_{Yb} and σ_{Tm} are the Allan deviations of the two clock lasers. The Allan deviation of the Yb^+ clock laser does not exceed 3×10^{-15} for the averaging times 0.5–50 s (with linear drift subtracted). The fractional instability produced by the fiber frequency doubler is less than 10^{-17} for an averaging time of 1 s [31]; therefore, the stability of 871 nm radiation is correctly transferred to 435.5 nm.

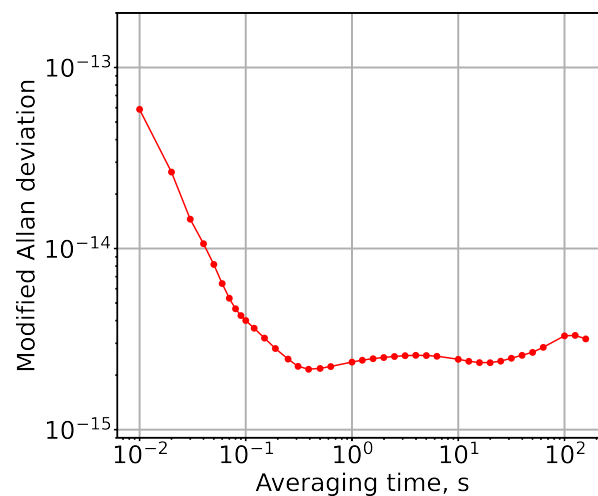


Figure 5. Modified Allan deviation σ_{beat} of the beat-note signal between 871 nm and OFC, stabilized by 1140 nm laser system. Linear drift of 348 mHz s^{-1} is subtracted.

3.3. Optical Frequency Comb

Transfer of the frequency stability of an optical clock to the microwave range is not possible without a precision frequency divider. In our case, we use an OFC based on a custom-developed, highly-stable femtosecond Er: fiber laser. The Avesta EFO-Comb was utilized to generate an IR frequency comb consisting of an array of narrow equidistant modes with frequencies $f = f_{ceo} + n \cdot f_{rep}$. The pulse repetition rate of the comb oscillator f_{rep} was set to 100 MHz and stabilized using the classic feedback approach, which is based on locking the optical frequency of a select comb tooth to that of the ytterbium optical clock output using a dedicated phase-lock loop (PLL). The offset frequency of the comb f_{ceo} , as determined by an F-2F interferometer was kept stable at 20 MHz by another PLL system operating independently from the f_{rep} PLL. Since our frequency comb cannot provide an offset-free spectrum due to $f_{ceo} \neq 0$, the design of the system made it possible to lock the offset frequency to a subharmonic of the pulse repetition rate. This ultimately resulted in a controlled carrier-envelope phase evolution of the output pulse train of the frequency comb. This way, if $f_{rep} = N \cdot f_{ceo}$ holds true with the help of a frequency divider or a local microwave oscillator (DDS), every N-th pulse of the train has the same absolute phase of the optical carrier. In our $^{171}\text{Yb}^+$ clock system, a frequency comb including a DDS and a set of frequency dividers to ensure assembly of $N = 5$.

The newly developed EFO-Comb had an all-PM design that included a femtosecond Er: fiber oscillator based on a nonlinear amplifying loop mirror (NALM) [32] configuration that ensures sufficient Kerr nonlinearity for continuous mode-locking and self-starting behavior. The active fiber was spliced into the loop section of the oscillator cavity coupled

with a free-space linear section that was used to house the f_{rep} and f_{ceo} servo mechanisms of the comb. The free-space section contained a LiNbO₃ crystal working as an electro-optic phase modulator, which was used to adjust the group delay of the passing pulse according to the high-pass filtered correction signal of the f_{rep} PLL. The low-frequency part of the f_{rep} correction signal was amplified and applied to a stack PZT actuator with the cavity end mirror mounted on its free side. In case the f_{rep} lock point drifted outside of the travel range of the PZT actuator ($\approx 10 \mu\text{m}$), e.g., in case of significant environmental changes, a stepper motor-assisted translation stage of the end mirror was automatically set in motion to eliminate the drift. Additionally, the large translation stage travel range of 15 mm proved itself useful for adjusting the spacing of the frequency comb's teeth so that two countable beat signals could be produced to phase-lock two arbitrary optical frequencies or compare the stability of two optical clocks with different wavelengths.

The offset frequency of the comb was controlled by injection current modulation of the oscillator pump diode and material dispersion dependent on the insertion depth of a pair of glass wedges located in the free-space section of the oscillator. The bandwidth of the fast f_{ceo} PLL channel acting via the current modulation was measured to be 110 kHz. The f_{ceo} PLL channel in control of the motorized wedge pair was used to compensate for the sub-Hz drifts of f_{ceo} , which were present due to variations in the ambient temperature and atmospheric pressure.

The output radiation of the stabilized Er: fiber oscillator was split evenly among several channels. One channel converted the optical signal of the comb into the electrical signal carrying the instantaneous value of f_{ceo} . This was achieved by first amplifying the 1560 nm output of the oscillator in a single-pass, two-way pumping the PM EDFA, compressing the resulting chirped pulses in a segment of the PM telecom fiber and, finally, feeding the compressed pulses into a supercontinuum generator providing an octave-spanning spectrum directly out of a highly nonlinear GeO₂-doped fiber. f_{ceo} could then be detected with well-established self-referencing techniques, for instance, using an F-2F interferometer. Another channel was used to directly shift the 1560 nm output of the oscillator to the target wavelength of 871 nm in order to reference it to the output of the Yb clock and optically lock the f_{rep} of the comb. This referencing involved combining the filtered 871 nm channel output of the frequency comb with the Yb optical clock's output in a typical Michelson interferometer arrangement and obtaining a beat note between the two. The beat-note frequency was then stabilized around 20 MHz with the aforementioned f_{rep} PLL. The optical part of the 871 nm channel was also based on the EDFA-compressor-supercontinuum generator setup with all its constituents optimized for effective coherent up-conversion of the 1560 nm output of the oscillator. Other channels of a similar design can be added to the frequency comb for wavelength stabilization of the Yb optical clock's cooling and excitation lasers, as well as generation of the narrow-band 1550 nm output used for locking the comb to a ULE cavity stabilized 1550 nm single-frequency laser in order to assess the accuracy of the frequency stability's transfer.

The output signal of the frequency comb paired with the Yb⁺ optical clock was produced by photodetecting the output pulse train of the comb after it passed through a factor of eight optical pulse-rate multiplier. A photodetector consisting of a fast PIN photodiode followed by an RF filtering circuit and amplifier produced a stable ultra-low phase noise microwave signal at 1 GHz, which can be distributed among the users.

In order to characterize the instability induced by optical-to-microwave conversion, we performed a comparison of two 1 GHz signals generated by identical detection modules. Each of the two photodetectors was connected to the output of the stabilized frequency comb through an independently adjustable attenuator. The outputs of the photodetectors were mixed on a pre-calibrated phase detector followed by a DC preamplifier and a low-pass filter producing an error signal that could later be digitized at a rate of at least 10 Hz by a digital voltmeter and stored on a PC. To ensure the linear operation of the phase detector outside of its dead zone, a short delay segment was introduced into one of the RF cables

connecting the photodetectors to the phase detector. The resulting phase difference data $\Delta\phi_i$ values were re-calculated into time difference values according to:

$$\Delta\tau_i = \frac{\Delta\phi_i}{2\pi F}, \quad (1)$$

where F is the RF carrier frequency equal to 1 GHz. Next, the fractional frequency data were obtained by the following:

$$\Delta f_i = \frac{\Delta\tau_{i+1} - \Delta\tau_i}{\tau_0}, \quad (2)$$

where τ_0 is the inverse sampling rate (i.e., 100 ms). The Allan deviation presented in Figure 6 demonstrates a fractional instability of an order of $1 \cdot 10^{-14}$ at 1 s observation time, $3 \cdot 10^{-16}$ at 100 s and less than $2 \cdot 10^{-17}$ at longer time periods (e.g., 1 h).

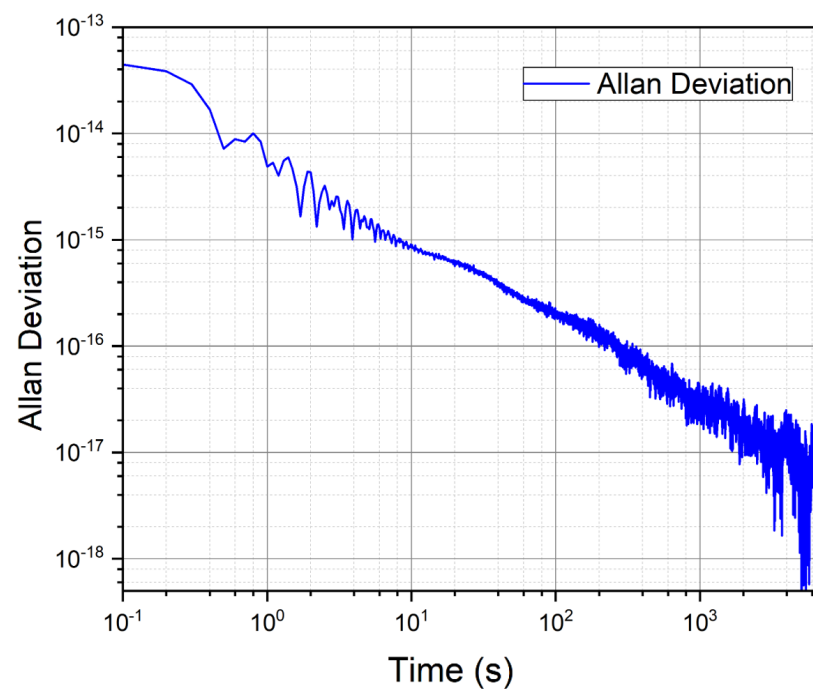


Figure 6. Allan deviation of two 1 GHz signals induced by optical-to-microwave conversion.

We estimated the resulting OFC-induced fractional instability of the $^{171}\text{Yb}^+$ optical clock's output signal at 1 GHz to be $9 \cdot 10^{-15}$ at 1 s, $1 \cdot 10^{-15}$ at 100 s and less than 10^{-16} at longer than an averaging time of 1000 s.

3.4. Spectroscopy of the Quadrupole Clock Transition

A single $^{171}\text{Yb}^+$ ion from a thermal atomic beam was loaded into the Paul trap by laser isotope selective photoionization. Doppler cooling was performed by driving the strong $^2S_{1/2} \rightarrow ^2P_{1/2}$ transition at 369.5 nm (Figure 7). The re-pumper at 935 nm returns an ion back to the cooling cycle in the case of $^2P_{1/2}$ state decay to the long-living $^2D_{3/2}$ state. To avoid population trapping in the hyperfine sublevels not involved in cooling, the 369 and 935 nm lasers were phase modulated by electro-optic modulators (EOMs) at frequencies of 14.7 and 3.07 GHz, respectively. Additionally, a static magnetic field of 500 μT was applied to destabilize the dark states appearing due to coherent population trapping [33]. After cooling (5 ms), modulation at a frequency of 14.7 GHz was switched off, and modulation at a frequency of 2.1 GHz was switched on using another electro-optic modulator placed in the same beam. This procedure prepared the initial clock transition state at a time of about 5 μs .

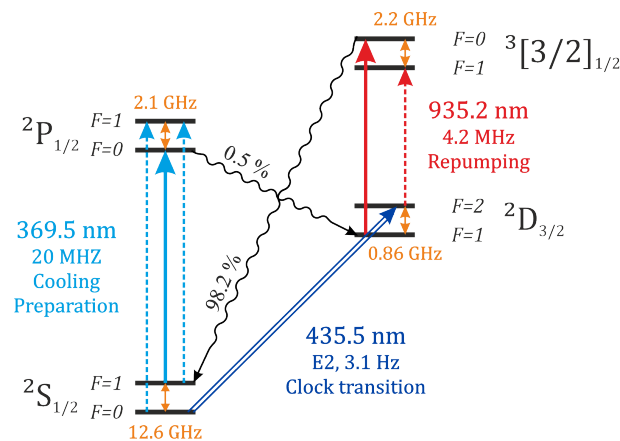


Figure 7. The $^{171}\text{Yb}^+$ ion level scheme (not to scale).

The readout of the clock transition excitation was performed by detecting the fluorescence signal of the ion at 369 nm. The cooling laser radiation was modulated at a frequency of 14.7 GHz; the EOM on 3.07 GHz of 935 nm radiation was switched off. The ion in the state $^2S_{1/2}$ ($F = 0$) efficiently scatters the photons collected using a 1-inch diameter aspherical lens on a photomultiplier tube (PMT) during 5 ms. If the ion is in the upper state $^2D_{3/2}$ ($F = 2$), fluorescence is absent, and only background photons or dark counts are detected on the PMT. The fidelity of initialization of the preparation and readout of the clock state of the setup is 98% if non-resonant excitation effects are neglected [34]. Figure 8 shows the spectrum of the clock transition upon the excitation by 30 ms π -pulses of the 435.5 nm laser. The approximation of the spectral line by a sinc function gives a width of 25 Hz, which corresponds to the Fourier limit and indicates that other types of broadening make minor contributions.

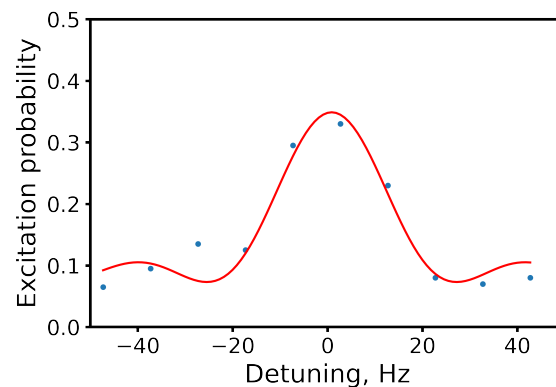


Figure 8. The clock transition excitation probability; π -pulse duration is 30 ms: (blue points) experimental data and (red line) the approximation by a sinc function.

4. Comparison with Tm Optical Clock

Characterization of the developed transportable $^{171}\text{Yb}^+$ single-ion clock was performed by comparison with the laboratory-based ^{69}Tm optical lattice clock [28]. The beat-note signal between the clock lasers was obtained similarly to the description in Section 3.2. The long-term stability of the clock laser systems at wavelengths of 871 nm and 1140 nm was provided by locking its frequency to the E2 and M1 ultra-narrow transitions in Yb and Tm, respectively. The beat-note signal was detected with the K+K FXE counter and analyzed using a modified Allan deviation. The instability of the 1 GHz signal was calculated as $\sigma_{result} = \sqrt{\sigma_{beat}^2 - \sigma_{Tm}^2 + \sigma_{conversion}^2}$, where σ_{beat} is the Allan deviation of the beat-note signal between the comb and the 871 laser, σ_{Tm} is the Allan deviation of the Tm

clock laser and $\sigma_{conversion}$ is the optical to radio-frequency conversion's instability, induced by the OFC. The result is presented in Table 1.

Table 1. The comparison between the developed transportable $^{171}\text{Yb}^+$ single-ion clock and the stationary ^{69}Tm optical lattice clock via the developed OFC.

Averaging Time	Signal Accumulation Time	σ_{Tm}	$\sigma_{conversion}$	σ_{beat}	σ_{result}
1 s	100 s	$2.7 \cdot 10^{-15}$	$8.5 \cdot 10^{-15}$	$3.7 \cdot 10^{-15}$	$8.9 \cdot 10^{-15}$
100 s	10,000 s	$6.1 \cdot 10^{-16}$	$2.1 \cdot 10^{-16}$	$1.1 \cdot 10^{-15}$	$9.4 \cdot 10^{-16}$
1000 s	24 h	$1.2 \cdot 10^{-16}$	$3.0 \cdot 10^{-17}$	$5.0 \cdot 10^{-16}$	$4.9 \cdot 10^{-16}$

5. New Solutions for Compact Clock Modules

5.1. Clock Laser with Low Sensitivity to Vibrations

Recently, a vast variety of transportable cavities and stabilized laser systems have been reported [35–39]. While the performance of the stationary systems benefits from using extra-long spacers [40] or cryogenic temperatures [41], transportable systems always operate at room temperature to improve their energy-saving capability and to be ready shortly after transportation; hence, the common principle for all mobile systems is utilizing ULE for the cavity body and ULE or fused silica for mirror substrates. Thus, the only ways to decrease the thermal noise limit include the enlarging of a cavity base or switching to crystalline mirror coatings [42]. Transportable ground or space systems are exposed to different continuous vibrations, or even huge overloads, during a rocket launch. This makes all-directional insensitivity to the accelerations inevitable, and, at the same time, the system should be fit for transportation. Thus, the next-generation system should be based on a reference cavity in which the suspension strategy provides fixation for all degrees of freedom. The first prototype of a clock laser system module was aimed at a significant mass-size reduction while keeping its performance, but the design of the reference cavity and its support system provided fixation and the lowest vibrational sensitivity only for the z-direction.

For the next generation of compact optical clocks, we propose a simple cavity spacer with the shape of a chamfered rectangle of the dimensions $100 \times 50 \times 50$ mm (Figure 9). The cavity will be based on stainless rods with a pair of Viton o-rings each for the preliminary experiments. This design makes it possible to change the bearing points easily, which makes the system more convenient for research.

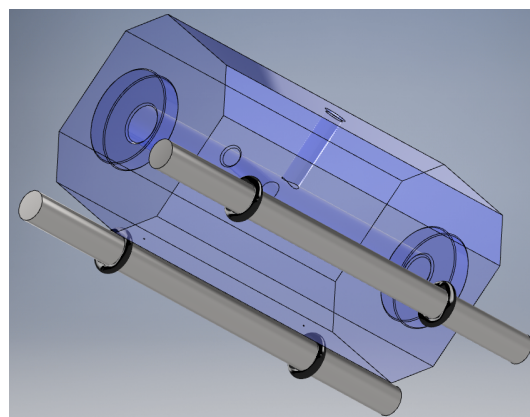


Figure 9. The next design of reference cavity with a part of the support system (bottom view; CAD drawing).

Such a support system provides constraints for the x- and y-axes as well. The bearing points were calculated to coincide with the Airy points. The depth of the chamber was

optimized with respect to the fractional length change, arising due to the unavoidable additional strain on the spacer produced by the force applied at each of the supports. The mirror substrates were made of Corning ULE: one is flat, and another is spherical with a 1000 mm radius of curvature. The reflective coating consists of a Bragg structure of 36 layers of $\text{SiO}_2/\text{Ta}_2\text{O}_5$, which provides a finesse of 225,000 (measured via ring-down, $\tau = 18.53$ us) with an on-resonant transmission of about 10%. The mirrors and the coatings were designed and manufactured at the P.N. Lebedev Physical Institute.

The cavity support, vacuum chamber and laser system layout are still under construction. We aim at a relative frequency instability lower than 5×10^{-15} for an averaging time from 0.1 to 100 s, a vibrational sensitivity lower than $10^{-10} [\frac{1}{g}]$ for all directions and a mass of the entire clock laser of less than 15 kg.

5.2. Compact OFC

For the first prototype, the entire optical scheme of the OFC was housed in an aluminum casing roughly the size of a standard 3U tall 19-inch rack-mountable unit. This optics unit was installed on a set of spring-loaded shock absorber mounts and attached to the frame of a transportable rack along with the rest of the modules comprising the atomic clock. The OFC electronics, including the laser power supply and control unit along with two PLL lockboxes and the DDS module, were put into four rack-mountable units with a total height of 9U. The electronic part of the comb was equipped with independent forced-air cooling built into the individual units, whereas the thermal stabilization of the optics unit was achieved with the help of thermoelectric coolers for the oscillator and a common breadboard of the casing, which also acted as a heat sink for other optical subassemblies within the optics unit.

The size and weight budget requirements of the OFC subsystem can be reduced by switching from the breadboard-based optics unit to an integrated design containing no dedicated mechanical subassemblies for various parts of the optical scheme and housing the entire optical scheme as a whole in a light, rigid, thermally stabilized container instead. The size and weight can be further reduced by replacing the free-space sections of the optical scheme, such as the F-2F interferometer and second harmonic generators, with fiber-based analogs. Further compactification of the frequency comb is possible via the integration of certain frequency comb electronics into standardized single-PCB modules based on their functional purposes and stacking such modules together into a tightly packaged unit that ensures efficient heat removal from the thermally loaded components. This approach makes it possible to scale down the OFC and improve its overall ruggedness and insensitivity to environmental perturbations, thus expanding the selection of available transportation options for the Yb^+ optical clock beyond the ground-based ones.

5.3. Planar Ion Trap with Elements of Integrated Photonics

For the next generation of the ion optical clock, we consider two approaches to ion traps. First is the development of traditionally used 3D traps with a magnetic shield and low heating rates. Another is a prospective chip-based surface trap with electrodes located in one plane. This architecture also has the advantage of optical access to the stored ion since the ions are trapped above the surface of the trap. This makes it possible to direct radiation from different laser systems onto an ion and to collect the fluorescence photons with a higher probability.

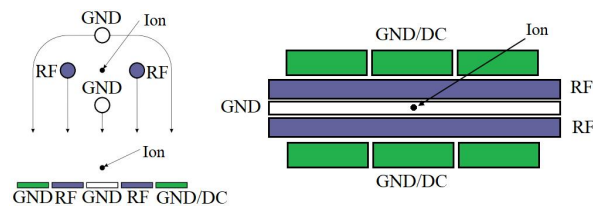


Figure 10. The planar ion trap with the surface electrodes from the side view with comparison to a 3D rod electrode trap (left) and the top view (right).

The stripe of the ground electrode is located between two also stripe-shaped RF electrodes as shown in Figure 10. The segmented electrodes on both sides of the RF electrodes are applied with a DC voltage and serve to hold the ions in the axial direction and compensate for the secular motions of the ions. All electrodes are located on the top of the dielectric substrate.

The main advantage of switching from the common 3D design to the planar trap design in the field of the optical clock is that this architecture is very friendly for merging with integrated photonic circuit (PIC) technologies, which can help minimize the size of the whole system and make it much more robust and convenient to use, as shown in Figure 11.

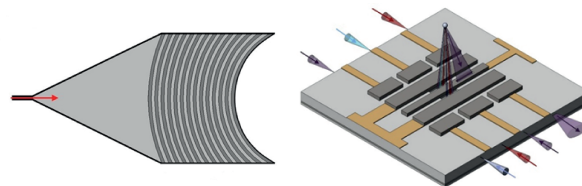


Figure 11. Schematic picture of the focusing grating coupler (left) and the planar trap with light delivery and detection using the PIC grating couplers (right) [43].

Switching to the miniaturized surface traps and a PIC will make it possible to use very compact full-metal vacuum chambers, as shown in Figure 12. Such a new design is advanced in comparison to those used before [44,45] due to a significant reduction in the internal volume and avoidance of the usage of complicated and expensive parts and components, such as ion pumps, massive optics, etc.

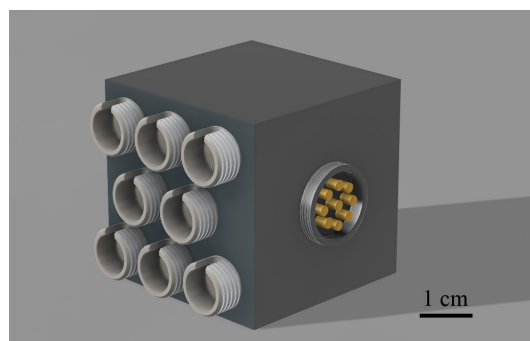


Figure 12. Schematic picture of the compact vacuum chamber.

5.4. Outlook

The next step to further improve our system and make it suitable for space applications is the development of a compact laser that is insensitive to vibrations, radiation and temperature fluctuations. Future designs might be based on narrow-linewidth diode laser sources based on integrated photonics that combine optical feedback with frequency stabilization to a reference cavity [46]. A space-grade diode laser source should be compact and have a long enough lifetime under extreme temperatures and radiation; therefore, an additional search for a light-emitting semiconductor structure design in order to increase

its overall efficiency is necessary [47]. Laser systems that perform ion cooling and pumping should be made all-fiber to avoid additional alignment while operating. We also plan to combine such a laser system with an ion trap based on integrated photonics, which is essential for further increasing system robustness while making the system more compact.

6. Conclusions

We presented LPI's first prototype $^{171}\text{Yb}^+$ transportable optical clock setup. The system is compact, robust and simple; it consists of separate modules and can easily start up after transportation. We performed a clock E2 transition at 435.5 nm spectroscopy with a typical line of 25 Hz. The fractional instability of the $^{171}\text{Yb}^+$ optical clock's first prototype developed in LPI is estimated to be less than 5×10^{-16} for an averaging time of $t > 10^4$.

This work is one of the many legacies of N.G. Basov's pioneering discoveries. Celebrating his 100th anniversary, we expect further development of this interesting branch of physics. Our work is a confirmation of the relevance and development of his work at his native institute—the Lebedev Physical Institute.

Author Contributions: Conceptualization, N.K. and K.K.; methodology, K.K. and I.S. (Ilya Semerikov); software, I.Z.; validation, A.B., D.K. and I.S. (Ilya Semerikov); investigation, A.B., I.S. (Ivan Sherstov) and I.Z.; data curation, A.B., D.K., I.Z. and A.T.; writing—original draft preparation, K.K., A.B., D.K., A.T. and T.A.; writing—review and editing, K.K. and D.K.; visualization, M.A. and I.S. (Ivan Sherstov); supervision, N.K.; project administration, K.K. All authors have read and agreed to the published version of the manuscript.

Funding: This research was funded by the Russian Ministry of Education and Science (ID no. RFMEFI61017X0010, agreement no. 14.610.21.0010).

Informed Consent Statement: Not applicable.

Data Availability Statement: The raw data can be provided upon request.

Acknowledgments: We are grateful to V. V. Belyaev for his contribution to engineering some mechanical parts of the system.

Conflicts of Interest: The authors declare no conflict of interest.

Abbreviations

The following abbreviations are used in this manuscript:

UTC	Coordinated Universal Time
TAI	International Atomic Time
OFC	Optical Frequency Comb
AC	Alternating Current
PDH	Pound–Drever–Hall
RF	Radio Frequency
DC	Direct Current
ECDL	External Cavity Diode Laser
FWHM	Full-Width Half-Maximum
ULE	Ultra-Low Expansion Glass
CTE	Coefficient of Thermal Expansion
PLL	Phase-Locked Loop
NALM	Nonlinear Amplifying Loop Mirror
DDS	Direct Digital Synthesis
PZT	Lead Zirconate Titanate
PM	Polarization Maintaining
EDFA	Erbium-Doped Fiber Amplifier
PC	Personal Computer
EOM	Electro-optic Modulator
AOM	Acousto-optic Modulator
PMT	Photomultiplier Tube
PIC	Integrated Photonic Circuits

References

1. Basov, N.G.; Letokhov, V.S. Optical frequency standards. *Sov. Phys. Uspekhi* **1969**, *11*, 855. [[CrossRef](#)]
2. Hinkley, N.; Sherman, J.A.; Phillips, N.B.; Schioppo, M.; Lemke, N.D.; Beloy, K.; Pizzocaro, M.; Oates, C.W.; Ludlow, A.D. An atomic clock with 10^{-18} instability. *Science* **2013**, *341*, 1215–1218. [[CrossRef](#)]
3. Sanner, C.; Huntemann, N.; Lange, R.; Tamm, C.; Peik, E.; Safronova, M.S.; Porsev, S.G. Optical clock comparison for Lorentz symmetry testing. *Nature* **2019**, *567*, 204–208. [[CrossRef](#)]
4. Mattingly, D. Modern tests of Lorentz invariance. *Living Rev. Relativ.* **2005**, *8*, 5. [[CrossRef](#)]
5. Matveev, A.; Parthey, C.G.; Predehl, K.; Alnis, L.; Beyer, A.; Holzwarth, R.; Udem, T.; Wilken, T.; Kolachevsky, N.; Abgrall, M. et al. Precision Measurement of the Hydrogen 1S-2S Frequency via a 920-km Fiber Link. *Phys. Rev. Lett.* **2013**, *110*, 230801. [[CrossRef](#)]
6. Safronova, M.S.; Budker, D.; DeMille, D.; Kimball, D.F.J.; Derevianko, A.; Clark, C.W. Search for new physics with atoms and molecules. *Rev. Mod. Phys.* **2018**, *90*, 025008. [[CrossRef](#)]
7. Udem, T.; Holzwarth, R.; Hänsch, T.W. Optical frequency metrology. *Nature* **2002**, *416*, 233–237. [[CrossRef](#)]
8. Origlia, S.; Pramod, M.S.; Schiller, S.; Singh, Y.; Bongs, K.; Schwarz, R.; Al-Masoudi, A.; Dörscher, S.; Herbers, S.; Häfner, S. et al. Towards an optical clock for space: Compact, high-performance optical lattice clock based on bosonic atoms. *Phys. Rev. A* **2018**, *98*, 053443. [[CrossRef](#)]
9. Hannig, S.; Pelzer, L.; Scharnhorst, N.; Kramer, J.; Stepanova, M.; Xu, Z.T.; Spethmann, N.; Leroux, I.D.; Mehlstäubler, T.E.; Schmidt, P.O. Towards a transportable aluminium ion quantum logic optical clock. *Rev. Sci. Instrum.* **2019**, *90*, 053204. [[CrossRef](#)]
10. Ohmae, N.; Takamoto, M.; Takahashi, Y.; Kokubun, M.; Araki, K.; Hinton, A.; Ushijima, I.; Muramatsu, T.; Furumiya, T.; Sakai, Y. et al. Transportable Strontium Optical Lattice Clocks Operated Outside Laboratory at the Level of 10^{-18} Uncertainty. *Adv. Quantum Technol.* **2021**, *4*, 2100015. [[CrossRef](#)]
11. Bize, S.; Laurent, P.; Abgrall, M.; Marion, H.; Maksimovic, I.; Cacciapuoti, L.; Grünert, J.; Vian, C.; Pereira dos Santos, F.; Rosenbusch, P. et al. Advances in atomic fountains. *Comptes Rendus Phys.* **2004**, *5*, 829–843. [[CrossRef](#)]
12. McGrew, W.F.; Zhang, X.; Fasano, R.J.; Schäffer, S.A.; Beloy, K.; Nicolodi, D.; Brown, R.C.; Hinkley, N.; Milani, G.; Schioppo, M. et al. Atomic clock performance enabling geodesy below the centimetre level. *Nature* **2018**, *564*, 87–90. [[CrossRef](#)] [[PubMed](#)]
13. Grotti, J.; Koller, S.; Vogt, S.; Häfner, S.; Sterr, U.; Lisdat, C.; Denker, H.; Voigt, C.; Timmen, L.; Rolland, A. et al. Geodesy and metrology with a transportable optical clock. *Nat. Phys.* **2018**, *14*, 437–441. [[CrossRef](#)]
14. Bothwell, T.; Kennedy, C.J.; Aeppli, A.; Kedar, D.; Robinson, J.M.; Oelker, E.; Staron, A.; Ye, J. Resolving the gravitational redshift across a millimetre-scale atomic sample. *Nature* **2022**, *602*, 420–424. [[CrossRef](#)] [[PubMed](#)]
15. Zheng, X.; Dolde, J.; Lochab, V.; Merriman, B.N.; Li, H.; Kolkowitz, S. Differential clock comparisons with a multiplexed optical lattice clock. *Nature* **2022**, *602*, 425–430. [[CrossRef](#)]
16. Koller, S.B.; Grotti, J.; Vogt, S.; Al-Masoudi, A.; Dörscher, S.; Häfner, S.; Sterr, U.; Lisdat, C. Transportable optical lattice clock with 7×10^{-17} uncertainty. *Phys. Rev. Lett.* **2017**, *118*, 073601. [[CrossRef](#)] [[PubMed](#)]
17. Cao, J.; Zhang, P.; Shang, J.; Cui, K.; Yuan, J.; Chao, S.; Wang, S.; Shu, H.; Huang, X. A compact, transportable single-ion optical clock with 7.8×10^{-17} systematic uncertainty. *Appl. Phys. B* **2017**, *123*, 112. [[CrossRef](#)]
18. Wolf, P.; Salomon, C.; Reynaud, S. Space clocks to test relativity: ACES and SAGA. *Proc. Int. Astron. Union* **2009**, *S261*, 377–389. [[CrossRef](#)]
19. Schiller, S.; Tino, G.M.; Gill, P.; Salomon, C.; Sterr, U.; Peik, E.; Nevsky, A.; Görlitz, A.; Svehla, D.; Ferrari, G. et al. Einstein Gravity Explorer—a medium-class fundamental physics mission. *Exp. Astron.* **2009**, *23*, 573–610. [[CrossRef](#)]
20. Origlia, S.; Schiller, S.; Pramod, M.S.; Smith, L.; Singh, Y.; He, W.; Viswam, S.; Świerad, D.; Hughes, J.; Bongs, K. et al. Development of a strontium optical lattice clock for the SOC mission on the ISS. *Quantum Opt.* **2016**, *9900*, 9–20.
21. Huntemann, N.; Sanner, C.; Lipphardt, B.; Tamm, Chr.; Peik, E. Single-ion Atomic Clock with 3×10^{-18} Systematic Uncertainty. *Phys. Rev. Lett.* **2016**, *116*, 063001. [[CrossRef](#)] [[PubMed](#)]
22. Zalivako, I.; Semerikov, I.; Borisenko, A.; Smirnov, V.; Vishnyakov, P.; Aksenov, M.; Sidorov, P.; Kolachevsky, N.; Khabarova, K. Improved wavelength measurement of $^2S_{1/2} \rightarrow ^2P_{1/2}$ and $^2D_{3/2} \rightarrow ^3[3/2]_{1/2}$ transitions in Yb^+ . *JRLR* **2019**, *40*, 375–381. [[CrossRef](#)]
23. Drever, R.W.P.; Hall, J.L.; Kowalski, F.V.; Hough, J.; Ford, G.M.; Munley, A.J.; Ward, H. Laser phase and frequency stabilization using an optical resonator. *Appl. Phys. B* **1983**, *31*, 97. [[CrossRef](#)]
24. Semerikov, I.A.; Zalivako, I.V.; Borisenko, A.S.; Aksenov, M.D.; Vishnyakov, P.A.; Sidorov, P.L.; Kolachevsky, N.N.; Khabarova, K.Yu. Three-dimensional Paul trap with high secular frequency for compact optical clock. *Bull. LPI* **2019**, *46*, 297–300. [[CrossRef](#)]
25. Alnis, J.; Matveev, A.; Kolachevsky, N.; Udem, T.; Hänsch, T.W. Subhertz linewidth diode lasers by stabilization to vibrationally and thermally compensated ultralow-expansion glass Fabry-Perot cavities. *Phys. Rev. A At. Mol. Opt. Phys.* **2008**, *77*, 1. [[CrossRef](#)]
26. Zhadnov, N.O.; Kudiyarov, K.S.; Kryuchkov, D.S.; Semerikov, I.A.; Khabarova, K.Yu.; Kolachevsky, N.N. On the thermal noise limit of ultrastable optical cavities. *Quantum Electron.* **2018**, *48*, 425. [[CrossRef](#)]
27. Zalivako, I.V.; Semerikov, I.A.; Borisenko, A.S.; Aksenov, M.D.; Vishnyakov, P.A.; Sidorov, P.L.; Semenin, N.V.; Golovizin, A.A.; Khabarova, K.Yu.; Kolachevsky, N.N. Compact ultrastable laser system for spectroscopy of $^2S_{1/2} \rightarrow ^2D_{3/2}$ quadrupole transition in 171Yb^+ ion. *Quantum Electron.* **2020**, *50*, 850. [[CrossRef](#)]
28. Golovizin, A.; Fedorova, E.; Tregubov, D.; Sukachev, D.; Khabarova, K.; Sorokin, V.; Kolachevsky, N. Inner-shell clock transition in atomic thulium with a small black body radiation shift. *Nat. Commun.* **2019**, *10*, 1. [[CrossRef](#)]
29. Carleton, H.R.; Maloney, W.T. A Balanced Optical Heterodyne Detector. *Appl. Opt.* **1968**, *7*, 1241–1243. [[CrossRef](#)]
30. Riehle, F. Optical clock networks. *Nat. Photonics* **2017**, *11*, 25. [[CrossRef](#)]

31. Delehaye, M.; Millo, J.; Bourgeois, P.-Y.; Groult, L.; Boudot, R.; Rubiola, E.; Bigler, E.; Kersalé, Y.; Lacroûte, C. Residual phase noise measurement of optical second harmonic generation in PPLN waveguides. *IEEE Photonics Technol. Lett.* **2017**, *29*, 1639. [[CrossRef](#)]
32. Fermann, M.E.; Haberl, F.; Hofer, M.; Hochreiter, H. Nonlinear amplifying loop mirror. *Opt. Lett.* **1990**, *15*, 752–754. [[CrossRef](#)] [[PubMed](#)]
33. Berkel, D.J.; Boshier, M.G. Destabilization of dark states and optical spectroscopy in Zeeman-degenerate atomic systems. *Phys. Rev. A* **2002**, *65*, 13.
34. Zalivako, I.V.; Semerikov, I.A.; Borisenko, A.S.; Aksenov, M.D.; Khabarova, K.Y.; Kolachevsky, N.N. Experimental Study of the Optical Qubit on the 435-nm Quadrupole Transition in the $^{171}\text{Yb}^+$ Ion. *JETP Lett.* **2021**, *114*, 59–64. [[CrossRef](#)]
35. Leibrandt, D.R.; Bergquist, J.C.; Rosenband, T. Cavity-stabilized laser with acceleration sensitivity below 10^{-12} g^{-1} . *Phys. Rev. A* **2013**, *87*, 3572–3574.
36. Chen, X.; Jiang, Y.; Li, B.; Yu, H.; Jiang, H.; Wang, T.; Yao, T.; Ma, L. Laser frequency instability of 6×10^{-16} using 10-cm-long cavities on a cubic spacer. *Chin. Opt. Lett.* **2020**, *18*, 030201. [[CrossRef](#)]
37. Argence, B.; Prevost, E.; Lévêque, T.; Le Goff, R.; Bize, S.; Lemonde, P.; Santarelli, G. Prototype of an ultra-stable optical cavity for space applications. *Opt. Express* **2012**, *20*, 25409–25420. [[CrossRef](#)] [[PubMed](#)]
38. Chen, Q.-F.; Nevsky, A.; Cardace, M.; Schiller, S.; Legero, T.; Häfner, S.; Uhde, A.; Sterr, U. A compact, robust, and transportable ultra-stable laser with a fractional frequency instability of 1×10^{-15} . *Rev. Sci. Instrum.* **2014**, *85*, 113107. [[CrossRef](#)]
39. Herbers, S.; Häfner, S.; Dörscher, S.; Lücke, T.; Sterr, U.; Lisdat, C. A transportable clock laser system with an instability of 1.6×10^{-16} . *arXiv* **2022**, arXiv:2207.08679.
40. Häfner, S.; Falke, S.; Grebing, C.; Vogt, S.; Legero, T.; Merimaa, M.; Lisdat, C.; Sterr, U. 8×10^{-17} fractional laser frequency instability with a long room-temperature cavity. *Opt. Lett.* **2015**, *40*, 2112–2115. [[CrossRef](#)]
41. Matei, D.G.; Legero, T.; Häfner, S.; Grebing, C.; Weyrich, R.; Zhang, W.; Sonderhouse, L.; Robinson, J.M.; Ye, J.; Riehle, F. et al. 1.5 m Lasers with Sub-10 mHz Linewidth. *Phys. Rev. Lett.* **2017**, *118*, 263202. [[CrossRef](#)]
42. Cole, G.D.; Zhang, W.; Martin, M.J.; Ye, J.; Aspelmeyer, M. Tenfold reduction of Brownian noise in high-reflectivity optical coatings. *Nat. Photonics* **2013**, *7*, 644–650. [[CrossRef](#)]
43. Abbasov, T.; Kazakov, I.; Sherstov, I.; Kontorov, S.; Shipulin, A.; Kueppers, F.; Lakhmanskiy, K. Focusing grating couplers for radio-frequency surface ion traps. In *Journal of Physics: Conference Series*; IOP Publishing: Bristol, UK, 2021; Volume 2015, p. 012001.
44. Niedermayr, D. Cryogenic Surface Ion Traps. Ph.D. Dissertation University of Innsbruck, Innsbruck, Austria, 2015.
45. Pearson, C.E. Theory and Application of Planar Ion Traps. Ph.D. Dissertation, University of Washington, Seattle, WA, USA, 2006.
46. Guo, J.; McLemore, C.A.; Xiang, C.; Lee, D.; Wu, L.; Jin, W.; Kelleher, M.; Jin, N.; Mason, D.; Chang, L. et al. Chip-Based Laser with 1 Hertz Integrated Linewidth. *arXiv* **2022**, arXiv:2203.16739.
47. Liu, B.; Xue, Q.; Yang, X.; Tan, S.T. Editorial: Advanced Nanomaterials for Light-Emitting Diodes and Solar Cells. *Front. Chem.* **2021**, *9*, 741760. [[CrossRef](#)] [[PubMed](#)]